Supporting Information for "On the relation between lithosphere thickness and surface heat flux for continental plume tracks"

Björn H. Heyn [1], Clinton P. Conrad [1]

[1]Centre for Earth Evolution and Dynamics (CEED), University of Oslo, Norway

Contents of this file

1. Text S1 to S2
2. Figures S1 to S3
3. Tables S1 to S4

Introduction This Supporting Information provides additional information required to reproduce the results shown in the paper. Text S1 describes the derivation of the analytical solution expressed in Eqs. (3) and (4) in the main text, and used in Figure 4. We include additional Figures S1-S3 to show how the relative heat flux anomaly behaves with non-dimensional length scale d (Figure S1), and the relative thinning Δh_{rel} (Figure S2), and show how the equilibration time changes with d and Δh_{rel} (Figure S3). Furthermore, Text S2 and Table S1 provides a more detailed description of the models and the parameters

necessary to run the simulations, and Tables S2-S4 give the data points shown in Figure 4.

Text S1. In order to derive an analytical solution for the temperature profile and the heat flux that follow instantaneous lithospheric thinning, we assume a stationary model, i.e. a model without convection. As a consequence, the temperature and heat flux change solely due to thermal conduction. For the initial undisturbed lithosphere, the equilibrated temperature profile in the lithosphere is given as

$$T(z,t) = T_0 + \frac{T_m - T_0}{L} z, \tag{1}$$

with the surface and LAB temperatures T_0 and T_m and the lithosphere thickness L. If we then thin lithosphere to a new thickness $l = L - \Delta h$ (see inlay in Figure 4) and let the system equilibrate for an infinite amount of time, the equilibrated temperature profile would be

$$T(z,t) = T_0 + \frac{T_m - T_0}{l} z. \tag{2}$$

Following the approach of Carslaw and Jaeger (1959) Chapter 3.4 for a case with initial temperature profile $f(x)$ and with ends kept at a fixed temperatures T_0 and T_m, we can split the solution into two parts $T(z,t) = u(z,t) + w(z,t)$, with $u(z,t)$ and $w(z,t)$ chosen

such that

$$\frac{d^2u}{dx^2} = 0$$

$$u(0,t) = T_0$$

$$u(l,t) = T_m$$

$$\frac{\partial w}{\partial t} = \kappa \frac{d^2w}{dx^2}$$

$$w(0,t) = w(l,t) = 0$$

$$w(z,0) = f(x) - u(z,0)$$

In our case, this translates to the boundary and initial conditions

$$T(0,t) = T_0 \tag{3}$$

$$T(l,t) = T_m \tag{4}$$

$$T(z,0) = T_0 + \frac{T_m - T_0}{L} z \qquad \text{(same as Equation (1))} \tag{5}$$

with the additional constraint that

$$T(z,\infty) = T_0 + \frac{T_m - T_0}{l} z \qquad \text{(same as Equation (2)).} \tag{6}$$

Using the solution for the linear temperature profile in Carslaw and Jaeger (1959) Chapter 3.3, which is

$$f(z) = kz = \sum_{n=1}^{\infty} a_n \sin\left(\frac{n\pi z}{l}\right) = \frac{2lk}{\pi} \sum_{n=1}^{\infty} \frac{(-1)^{n-1}}{n} \sin\left(\frac{n\pi z}{l}\right), \tag{7}$$

we find

$$u(z,t) = T_0 + \frac{T_m - T_0}{l} z$$

$$w(z,t) = -\frac{2lk}{\sum}_{n=1}^{\infty} \frac{(-1)^{n-1}}{n} \exp\left[\frac{-\kappa n^2 \pi^2}{l^2} t\right] \sin\left(\frac{n\pi z}{l}\right)$$

with thermal diffusivity κ. Finally, we can then express the temperature profile as a function of time and depth via

$$T(z,t) = T_0 + \frac{T_m - T_0}{l} z - \frac{2lk}{\pi} \sum_{n=1}^{\infty} \frac{(-1)^{n-1}}{n} \exp\left[-\frac{\kappa n^2 \pi^2}{l^2} t\right] \sin\left(\frac{n\pi z}{l}\right). \tag{8}$$

Our temperature gradient k is the differential gradient between Equations (1) and (2) and can be calculated via

$$\begin{aligned} k = \frac{\Delta T}{l} &= \frac{T_m - T^*}{l} = \frac{1}{l}\left(T_m - T_0 - \frac{T_m - T_0}{L} l\right) = \frac{1}{l}(T_m - T_0)(1 - \frac{l}{L}) \\ &= (T_m - T_0)\left(\frac{1}{l} - \frac{1}{L}\right), \end{aligned}$$

with $T^* = T(l,0) = T_0 - \frac{T_m - T_0}{L} l$ from Equation (1).

With respect to our boundary and initial conditions (Equations (3)-(6)), we get

$$\begin{aligned} Eq.(3) : T(0,t) &= T_0 + \underbrace{\left(\frac{T_m - T_0}{l} 0\right)}_{=0} - \underbrace{\left(\frac{2lk}{\pi} \sum_{n=1}^{\infty} \frac{(-1)^{n-1}}{n} \exp\left[-\frac{\kappa n^2 \pi^2}{l^2} t\right] \sin\left(\frac{n\pi 0}{l}\right)\right)}_{=0} \\ &= T_0 \\ Eq.(4) : T(l,t) &= T_0 + \underbrace{\left(\frac{T_m - T_0}{l} l\right)}_{=T_m - T_0} - \underbrace{\left(\frac{2lk}{\pi} \sum_{n=1}^{\infty} \frac{(-1)^{n-1}}{n} \exp\left[-\frac{\kappa n^2 \pi^2}{l^2} t\right] \sin\left(\frac{n\pi l}{l}\right)\right)}_{=0} \\ &= T_m \\ Eq.(5) : T(z,0) &= T_0 + \left(\frac{T_m - T_0}{l} z\right) - \underbrace{\left(\frac{2lk}{\pi} \sum_{n=1}^{\infty} \frac{(-1)^{n-1}}{n} \exp\left[-\frac{\kappa n^2 \pi^2}{l^2} 0\right] \sin\left(\frac{n\pi z}{l}\right)\right)}_{\text{Eq. (7): } = kz = (T_m - T_0)\left(\frac{1}{l} - \frac{1}{L}\right) z} \\ &= T_0 + \frac{T_m - T_0}{L} z \\ Eq.(6) : \lim_{t\to\infty} T(z,t) &= T_0 + \left(\frac{T_m - T_0}{l} z\right) - \underbrace{\lim_{t\to\infty} \left(\frac{2lk}{\pi} \sum_{n=1}^{\infty} \frac{(-1)^{n-1}}{n} \exp\left[-\frac{\kappa n^2 \pi^2}{l^2} t\right] \sin\left(\frac{n\pi z}{l}\right)\right)}_{=0} \\ &= T_0 + \frac{T_m - T_0}{l} z \end{aligned}$$

In order to obtain the heat flux, we use the heat flux equation $q = -K\frac{dT}{dz}$ with thermal conductivity K

$$q(z,t) = \frac{T_m - T_0}{l} - 2k\sum_{n=1}^{\infty}(-1)^{n-1}\exp\left[-\frac{\kappa n^2\pi^2}{l^2}t\right]\cos\left(\frac{n\pi z}{l}\right)$$

At the surface ($z = 0$), this simplifies to

$$q(0,t) = \frac{T_m - T_0}{l} - 2k\sum_{n=1}^{\infty}(-1)^{n-1}\exp\left[-\frac{\kappa n^2\pi^2}{l^2}t\right]. \tag{9}$$

We then introduce the non-dimensional length scale

$$d = 2\frac{\sqrt{\kappa t}}{l} \tag{10}$$

and express k in terms of relative thinning

$$k = (T_m - T_0)\left(\frac{1}{l} - \frac{1}{L}\right) = (T_m - T_0)\left(\frac{L-l}{Ll}\right)$$
$$\underbrace{=}_{L-l=\Delta h} \frac{T_m - T_0}{l}\Delta h_{rel}.$$

Using this, we can calculate the plume-induced heat flux anomaly $\Delta q = q - q_0$ relative to the undisturbed heat flux q_0 as

$$\begin{aligned}
\Delta q_{rel}(0,t) &= \frac{\Delta q}{q_0} = \frac{q}{q_0} - 1 \\
&= \frac{\frac{T_m-T_0}{l} - 2\frac{T_m-T_0}{l}\Delta h_{rel}\sum_{n=1}^{\infty}(-1)^{n-1}\exp\left[-\frac{n^2\pi^2}{4}d^2\right]}{\frac{T_m-T_0}{L}} - 1 \\
&= \frac{L}{l} - 2\frac{L}{l}\Delta h_{rel}\sum_{n=1}^{\infty}(-1)^{n-1}\exp\left[-\frac{n^2\pi^2}{4}d^2\right] - 1 \\
&= \Delta h_{rel}\frac{L}{l} - 2\frac{L}{l}\Delta h_{rel}\sum_{n=1}^{\infty}(-1)^{n-1}\exp\left[-\frac{n^2\pi^2}{4}d^2\right] \\
&= \Delta h_{rel}\frac{L}{l}\left(1 - 2\sum_{n=1}^{\infty}(-1)^{n-1}\exp\left[-\frac{n^2\pi^2}{4}d^2\right]\right) \\
\Delta q_{rel}(0,t) &= \frac{\Delta h_{rel}}{1-\Delta h_{rel}}\left(1 - 2\sum_{n=1}^{\infty}(-1)^{n-1}\exp\left[-\frac{n^2\pi^2}{4}d^2\right]\right).
\end{aligned} \tag{11}$$

Here, we used the relations

$$\frac{L}{l} - 1 = \frac{L-l}{l} \cdot \frac{L}{L} = \frac{L-l}{L} \cdot \frac{L}{l} = \Delta h_{rel} \frac{L}{l} \qquad \text{and}$$
$$\Delta h_{rel} \frac{L}{l} = \frac{\Delta h_{rel}}{\frac{l}{L}} = \frac{\Delta h_{rel}}{\frac{L}{L} - \frac{L-l}{l}} = \frac{\Delta h_{rel}}{1 - \Delta h_{rel}}.$$

In the limits of $t \to 0$ and $t \to \infty$ (and thus $d \to 0$ and $d \to \infty$), we obtain the heat flux anomalies

$$\begin{aligned} \Delta q_{rel}(0, t \to 0) &= \frac{\Delta h_{rel}}{1 - \Delta h_{rel}} \left(1 - 2 \underbrace{\sum_{n=1}^{\infty} (-1)^{n-1} \exp\left[-\frac{n^2 \pi^2}{4} d^2 \right]}_{=1/2} \right) \\ &= 0 \end{aligned} \tag{12}$$

$$\begin{aligned} \Delta q_{rel}(0, t \to \infty) &= \frac{\Delta h_{rel}}{1 - \Delta h_{rel}} \left(1 - 2 \underbrace{\lim_{d \to \infty} \sum_{n=1}^{\infty} (-1)^{n-1} \exp\left[-\frac{n^2 \pi^2}{4} d^2 \right]}_{=0} \right) \\ &= \frac{\Delta h_{rel}}{1 - \Delta h_{rel}} \end{aligned} \tag{13}$$

Note, however, that Δq_{rel} is not well defined exactly at $t = 0$, since the exponential part of the sum in Eq. (12) at that time would yield $\exp\left[-\frac{n^2 \pi^2}{4} 0^2 \right] = 1$, and the sum does not converge in this case. Convergence for $t \to 0$ can be seen either by numerically calculating the sum over the first few thousand elements for very small t, or by "visualizing" the first few elements of the sum in an approximate way: for $n = 1$, the sum element is positive and close to 1, for $n = 2$ the element is negative and slightly smaller than the previous element due to the exponential decay. $n = 3$ yields a positive element again, but smaller than the previous ones, and so it continues. For increasing n, the elements get smaller due to the exponential decay, while every odd n gives a positive and every even n a negative

contribution. This means the sum should converge to a value of 0.5, which is exactly the same result we obtain for the numerical approach.

Figure S1 shows the evolution of the relative heat flux anomaly (Eq. (11)) versus d (and thus versus (the square root of) time, compare Eq. (10)) for different values of relative lithosphere thinning. As can be seen, all curves asymptotically approach their maximum value before $d = 2$, although models with more thinning require more time to reach that maximum. The same behavior for d can be seen when plotting the relative heat flux anomaly Δq_{rel} versus the relative thinning Δh_{rel}, see Figure S2 and Figure 4 in the main text. Again, a value of $d = 2$ predicts basically the same anomalies as a value of $d \to \infty$ (shown as dashed line in Figure S2).

Finally, we can convert the value of d to a theoretical equivalent time it takes for a stationary model to develop the respective heat flux anomaly (Eq. (11), shown in Figures S1-S2) for a given lithosphere thinning Δh_{rel} via Equation (10):

$$\begin{aligned} t &= d^2 \frac{l^2}{4\kappa} = d^2 \frac{(L - \Delta h)^2}{4\kappa} \cdot \frac{L^2}{L^2} \\ &= d^2 \frac{L^2 (1 - \Delta h_{rel})^2}{4\kappa} \end{aligned} \tag{14}$$

As can be seen in Figure S3, the equivalent time required decreases with increasing lithosphere thinning (for constant d) or decreasing value of d (for constant lithosphere thinning).

For Figure 4 in the main text, we assumed a constant equilibration time, a constant value of $L = 137.8\,\text{km}$ and then used Equation (10) to calculate the corresponding value

of d depending on the relative thinning Δh_{rel}:

$$d = 2\frac{\sqrt{\kappa t}}{l} = 2\sqrt{\kappa t}\frac{1}{L-(L-l)} = 2\sqrt{\kappa t}\frac{1}{L-(L-l)} \cdot \frac{1}{\frac{L}{L}} = 2\sqrt{\kappa t}\frac{1}{L - L\frac{L-l}{L}}$$
$$= 2\sqrt{\kappa t}\frac{1}{L(1-\Delta h_{rel})}$$

This can be used as input to Equation (11) to obtain the lines for constant t shown in Figure 4.

Text S2. Our 2-D stationary plate models have domain sizes of 1200x600 km (x by z), 2-D moving plate cases are 5500x800 km (x by z) and 3-D moving plate cases are 5500x2000x800 km (x by y by z). Resolutions vary within the models due to adaptive mesh refinements, but range between 3 x 3 km to 25 x 2 km. The chosen box dimensions should ensure that all important plume-lithosphere interactions are captured and boundary effects are minimized, while keeping computational costs limited. The choice of Cartesian geometry does not significantly affect the results, since the Earth's curvature is minimal for the chosen box dimensions. For models with 3 cm/yr plate velocity, we had to increase the domain size to 5500x1100 km to prevent the temperature anomaly from being sheared at the bottom. The viscosity is implemented via equations (1) and (2) in the main text, with a step-wise implementation of depth-dependence via η_j. η_j is the scaling viscosity for the two layers we have: layer one ($j = 1$) reaching from the surface down to the bottom of the asthenosphere, and layer two ($j = 2$) for the domain below the asthenosphere.

The surface temperature is fixed to 273 K for all models at all time steps, while the LAB temperature (in the reference models at 150 km depth) is initially set to either 1500 K or

1623 K. Below the LAB, the initial temperature profile has a small temperature gradient to facilitate plume rise. Although the details of this gradient vary slightly between stationary (respective bottom temperatures of 1623 K or 1650 K) and moving plate cases (bottom temperatures of 1550 K and 1650 K) due to numerical stability of the solution, these choices do not significantly affect the results of plume-lithosphere interaction. At the bottom, we further add a temperature anomaly of Gaussian shape ($T_p \cdot \exp\left[-\frac{(x-s)^2}{2*w^2}\right]$) with plume excess temperature T_p, width $w = 500$ km for stationary plates ($w = 300$ km for moving plate cases) and shift $s = 600$ km ($s = 1500$ km for moving plates) to trigger and sustain a plume.

As mentioned in the main text, estimated buoyancy fluxes for our models are about 1 Mg/s for the 2-D and 3-D reference cases, and about 1.5 Mg/s for models with 400 K plume excess temperature. Although these fluxes are not as high as the largest ones observed on Earth (see e.g. Hoggard et al., 2020, and references therein), they fall well within the range of observations, which vary significantly between studies. However, despite the fact that the plume flux is a good way to measure and compare plume strength, we do not expect the amplitudes of heat flux and lithosphere thinning anomalies to scale directly with plume flux. Plume flux is calculated as the density anomaly times the rising velocity, integrated over a slice through the plume: $B = \int v_\mathrm{r} \rho \alpha T_P dS$, with density ρ, thermal expansivity α, plume excess temperature T_P, the vertical velocity v_r, and teh surface increment dS (Farnetani et al., 2018). For 2-D models, rotational symmetry of the temperature and rising velocity are assumed (compare Heyn et al., 2020). As a consequence, a change in plume flux can be related to a change in plume excess temperature, rising

velocity, or the diameter of the plume. While the excess temperature affects anomaly amplitudes (as discussed in the paper), a change in rising velocity may affect the plume's ability to mechanically erode the lithosphere, and therefore affects predicted anomalies. we expect the plume diameter, on the other hand, to primarily affect the width of the plume track, and will only minimally affect the amplitudes of lithosphere thinning and surface heat flux. Therefore, for this study, we consider that plume excess temperature is more important than plume buoyancy flux.

References

Carslaw, H. S., & Jaeger, J. C. (1959). *Conduction of heat in solids.* Oxford University Press.

Farnetani, C. G., Hofmann, A. W., Duvernay, T., & Limare, A. (2018). Dynamics of rheological heterogeneities in mantle plumes. *Earth and Planetary Science Letters*, *499*, 74–82. Retrieved from http://www.sciencedirect.com/science/article/pii/S0012821X1830428X doi: 10.1016/j.epsl.2018.07.022

Heyn, B. H., Conrad, C. P., & Trønnes, R. G. (2020). How thermochemical piles can (periodically) generate plumes at their edges. *Journal of Geophysical Research: Solid Earth*, *125*(6), e2019JB018726. Retrieved from https://agupubs.onlinelibrary.wiley.com/doi/abs/10.1029/2019JB018726 (e2019JB018726 10.1029/2019JB018726) doi: 10.1029/2019JB018726

Hoggard, M. J., Parnell-Turner, R., & White, N. (2020). Hotspots and mantle plumes revisited: Towards reconciling the mantle heat transfer discrepancy. *Earth and Planetary Science Letters*, *542*, 116317. Retrieved from https://www.sciencedirect

.com/science/article/pii/S0012821X20302612 doi: 10.1016/j.epsl.2020.116317

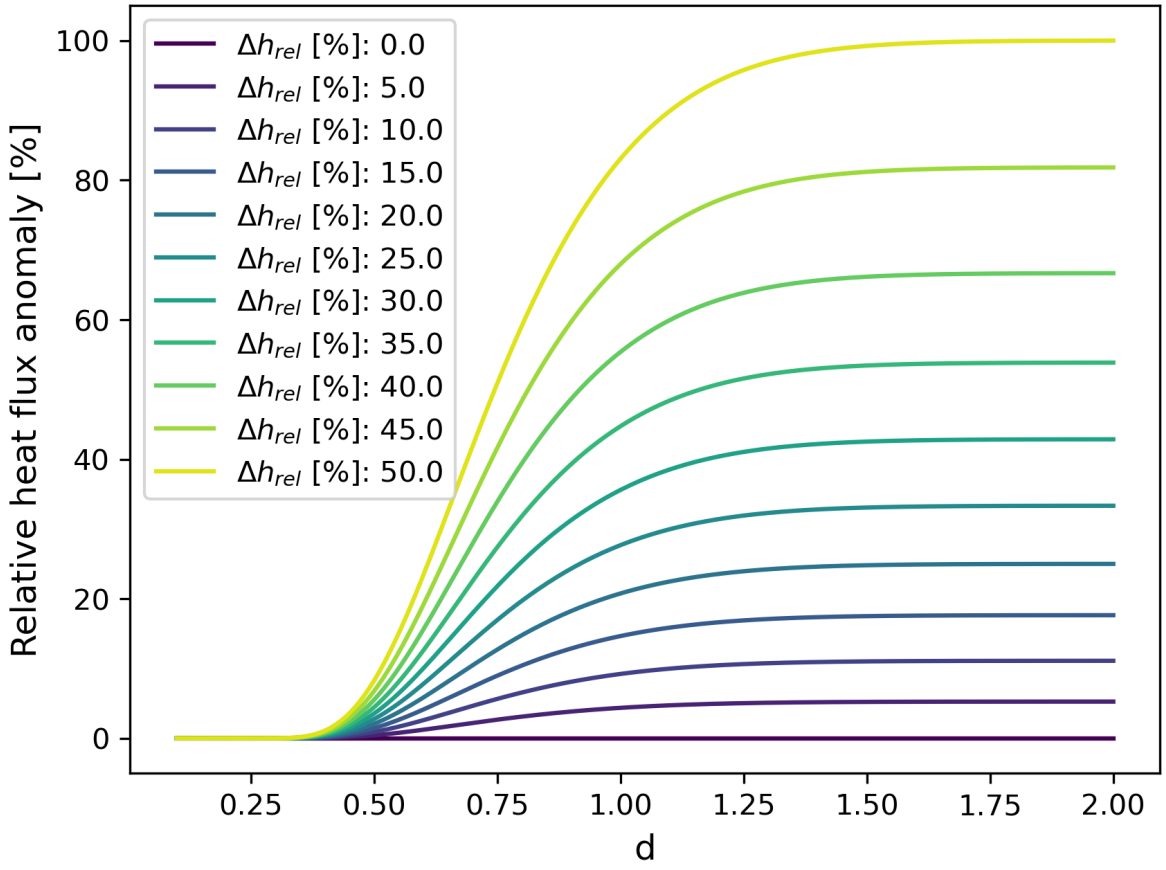

Figure S1. Relative heat flux anomaly as a function of d for different values of relative lithosphere thinning Δh_{rel}.

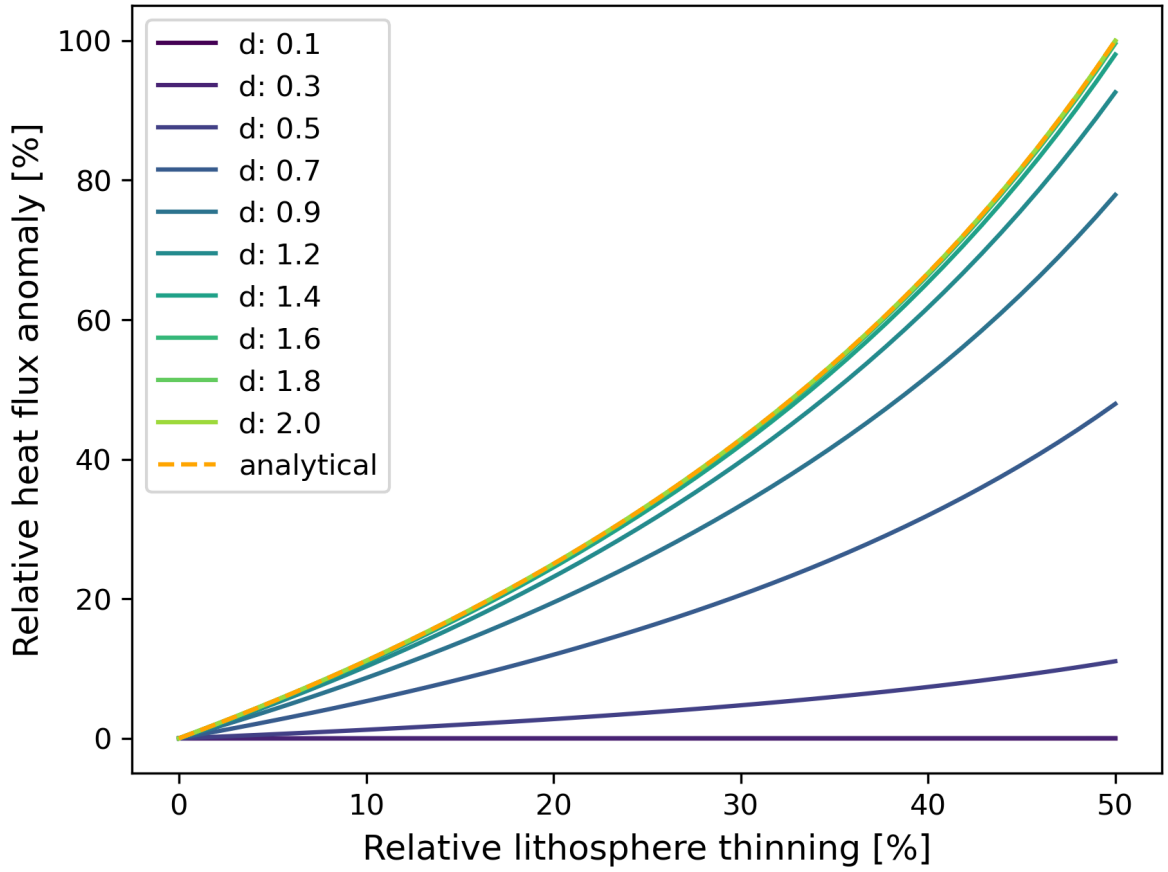

Figure S2. Relative heat flux anomaly as a function of relative lithosphere thinning Δh_{rel} for different choices of d. The analytical line assumes $d \to \infty$ (see Equation (13)).

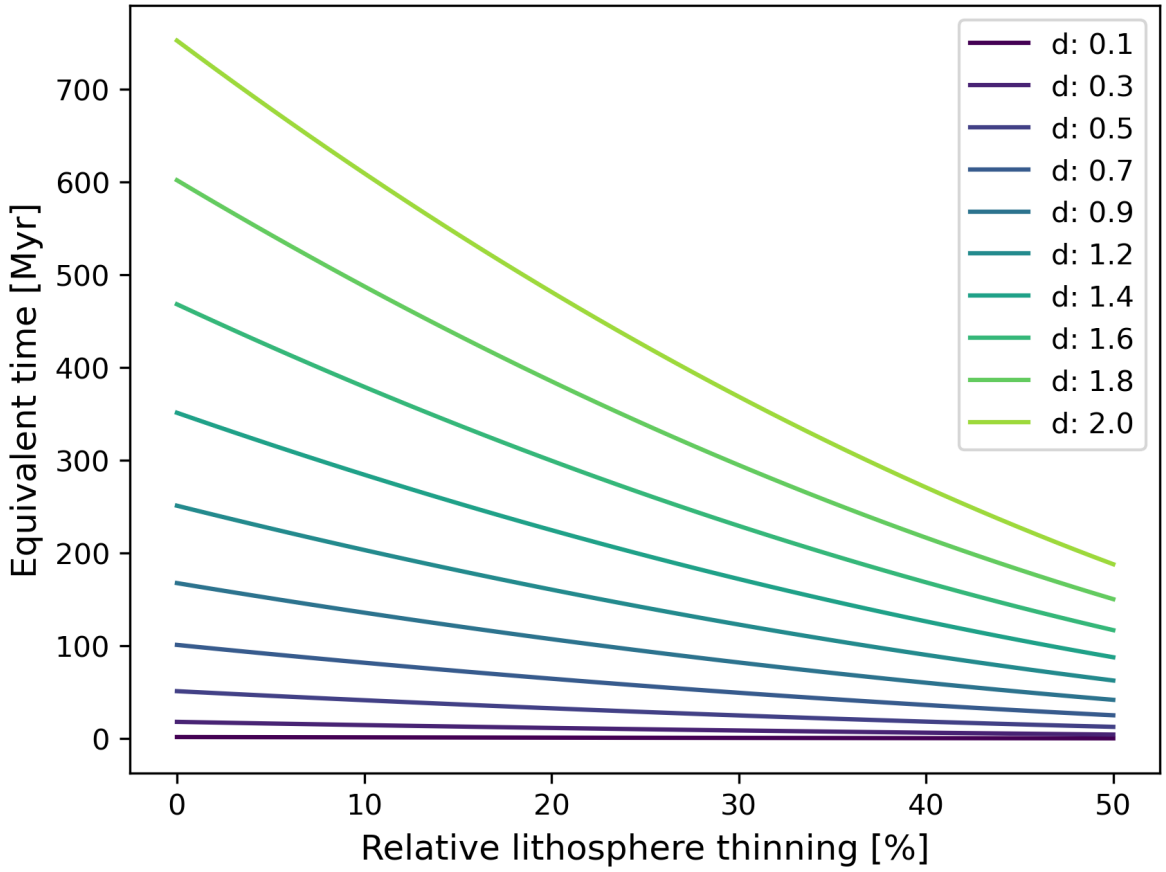

Figure S3. Equivalent time required to develop the corresponding heat flux anomaly (shown in Figure S2) as a function of relative lithosphere thinning Δh_{rel} for different choices of d and a constant $L = 137.8\,\mathrm{km}$. A value of $d < \infty$, but in practice $d < 2.0$, means that the system does not equilibrate to the maximum potential surface heat flux (compare Figure S1). Equivalent times are derived for a stationary model following Equation (14).

Table S1. Input parameters and their ranges for the numerical models. Only one of the 2-D stationary plate models has no dedicated low viscosity asthenosphere, otherwise we use a step function at the bottom of the asthenosphere to increase upper mantle viscosity relative to the asthenosphere viscosity. For models with diffusion-dislocation creep, we further set grain size $d = 1 \cdot 10^{-3}\,\mathrm{m}$, activation energies $E_{\mathrm{diff}} = 373\,\mathrm{kJ/mol}$ and $E_{\mathrm{disl}} = 530\,\mathrm{kJ/mol}$, activation volumes $V_{\mathrm{diff}} = 6{\cdot}10^{-6}\,\mathrm{m^3/mol}$ and $V_{\mathrm{disl}} = 1.4{\cdot}10^{-5}\,\mathrm{m^3/mol}$, grain size exponent $m = 3$, stress exponents $n_{\mathrm{diff}} = 1$ and $n_{\mathrm{disl}} = 3.5$, and viscosity prefactors $A_{\mathrm{diff}} = 1.5 \cdot 10^{15}\,\mathrm{m^3/(Pa{\cdot}s)}$ and $A_{\mathrm{disl}} = 1.1 \cdot 10^{16}\,(\mathrm{Pa^{-3.5}{\cdot}s^{-1}})$.

Parameter	Reference value	Range	Unit
Thermal diffusivity κ	$0.8 \cdot 10^{-6}$	–	$\mathrm{m^2/s}$
Reference density ρ	3300	–	$\mathrm{kg/m^3}$
Specific heat capacity c_p	1250	–	J/(kg·K)
Gravitational acceleration g	9.81	–	$\mathrm{m/s^2}$
Viscosity prefactor A	$8 \cdot 10^{-12}$	–	1/Pa·s
Thermal expansivity α	$3.5 \cdot 10^{-5}$	–	1/K
Constant radiogenic heating H	$7.58 \cdot 10^{-12}$	–	W/kg
Reference viscosity η_{ref}	$1 \cdot 10^{22}$	–	Pa·s
LAB temperature T_{LAB}	1500	$1500 - 1623$	K
Layer viscosity scalings η_j	$[5 \cdot 10^{22}, 1 \cdot 10^{24}]$	$[1 \cdot 10^{21} - 5 \cdot 10^{23}, 1 \cdot 10^{24}]$	Pa·s
Initial lithosphere thickness L	150	$100 - 200$	km
Asthenosphere thickness d_{Asth}	150	$0 - 200$	km
Asthenosphere viscosity η_{Asth}	$1 \cdot 10^{19}$	$5 \cdot 10^{17} - 1 \cdot 10^{20}$	Pa·s
Plume excess temperature T_p	250	$100 - 450$	K
Maximum lithosphere viscosity η_{max}	$1 \cdot 10^{29}$	$1 \cdot 10^{26} - 1 \cdot 10^{29}$	Pa·s
Plume life time t_p	200	$50 - 200$	Myr
Plate velocity v	1.5	$0.75 - 3.0$	cm/yr
Activation energy E	250	$100 - 300$	kJ/mol

Table S2. Overview of 2-D stationary plate models used to create the data in Figure 4. The first column defines which parameter(s) defined in Table S1 deviate from the reference values given in Table S1. The other columns are the maximum heat flux anomaly Δq (in $\mathrm{mW/m^2}$), the maximum lithospheric thinning Δh (in km), the reference heat flux q_0 at the time of maximum heat flux (in $\mathrm{mW/m^2}$), and the reference lithosphere thickness L at the time of maximum thinning (in km).

Changed parameter(s)	Δq	Δh	q_0	L
– (ref. case)	7.302	51.5	26.685	158.49
$t_p = 100\,\mathrm{Myr}$	4.016	40.6	24.909	175.98
$t_p = 50\,\mathrm{Myr}$	3.223	43.9	24.601	189.58
$T_p = 150\,\mathrm{K}$	5.680	53.1	25.122	173.84
$T_p = 200\,\mathrm{K}$	6.526	53.3	25.899	166.64
$T_p = 300\,\mathrm{K}$	8.097	49.2	27.459	150.97
$T_p = 400\,\mathrm{K}$	10.725	46.9	29.262	136.77
$d_{\mathrm{Asth}} = 0\,\mathrm{km}$	1.349	23.2	23.526	185.92
$d_{\mathrm{Asth}} = 100\,\mathrm{km}$	7.976	54.7	26.269	161.37
$d_{\mathrm{Asth}} = 100\,\mathrm{km}$, $t_p = 100\,\mathrm{Myr}$	4.150	41.8	26.521	161.83
$d_{\mathrm{Asth}} = 100\,\mathrm{km}$, $t_p = 50\,\mathrm{Myr}$	2.927	39.9	24.588	190.71
$L = 100\,\mathrm{km}$	9.231	47.8	31.059	139.50
$L = 100\,\mathrm{km}$, $t_p = 100\,\mathrm{Myr}$	4.745	34.9	33.531	166.96
$L = 100\,\mathrm{km}$, $t_p = 50\,\mathrm{Myr}$	2.890	33.1	27.104	173.92
$L = 200\,\mathrm{km}$	5.559	57.2	22.670	186.14
$L = 200\,\mathrm{km}$, $t_p = 100\,\mathrm{Myr}$	3.449	48.6	22.238	200.71
$L = 200\,\mathrm{km}$, $t_p = 50\,\mathrm{Myr}$	2.741	50.5	21.953	207.58
$E = 100\,\mathrm{kJ/mol}$	43.664	130.4	73.077	223.91
$E = 100\,\mathrm{kJ/mol}$, $t_p = 100\,\mathrm{Myr}$	33.518	130.4	61.354	223.91
$E = 150\,\mathrm{kJ/mol}$	25.209	36.9	45.511	99.35
$E = 150\,\mathrm{kJ/mol}$, $t_p = 100\,\mathrm{Myr}$	16.665	43.5	36.711	115.60
$E = 200\,\mathrm{kJ/mol}$	18.160	50.3	31.614	122.64
$E = 200\,\mathrm{kJ/mol}$, $t_p = 100\,\mathrm{Myr}$	11.355	51.7	29.117	144.90
$\eta_j = [5 \cdot 10^{21}, 1 \cdot 10^{24}]\,\mathrm{Pa{\cdot}s}$	16.314	49.6	31.179	125.72
$\eta_j = [5 \cdot 10^{23}, 1 \cdot 10^{24}]\,\mathrm{Pa{\cdot}s}$	2.159	31.5	24.177	180.62
$\eta_j = [5 \cdot 10^{23}, 1 \cdot 10^{24}]\,\mathrm{Pa{\cdot}s}$, $L = 100\,\mathrm{km}$	2.600	27.3	27.629	157.31
$\eta_j = [5{\cdot}10^{23}, 1{\cdot}10^{24}]\,\mathrm{Pa{\cdot}s}$, $L = 100\,\mathrm{km}$, $\eta_{\mathrm{max}} = 1{\cdot}10^{26}\,\mathrm{Pa{\cdot}s}$	2.601	27.3	27.616	157.32
$\eta_{\mathrm{max}} = 1 \cdot 10^{26}\,\mathrm{Pa{\cdot}s}$	7.345	52.2	26.638	159.14
$\eta_{\mathrm{max}} = 1 \cdot 10^{26}\,\mathrm{Pa{\cdot}s}$, $t_p = 100\,\mathrm{Myr}$	4.022	40.8	24.910	176.11
$\eta_{\mathrm{max}} = 1 \cdot 10^{26}\,\mathrm{Pa{\cdot}s}$, $t_p = 50\,\mathrm{Myr}$	3.231	44.9	24.590	190.58
$\eta_{\mathrm{max}} = 1 \cdot 10^{26}\,\mathrm{Pa{\cdot}s}$, $L = 100\,\mathrm{km}$	9.250	48.3	31.041	140.24
$\eta_{\mathrm{max}} = 1 \cdot 10^{26}\,\mathrm{Pa{\cdot}s}$, $L = 100\,\mathrm{km}$, $t_p = 100\,\mathrm{Myr}$	4.735	35.0	33.535	165.41
$\eta_{\mathrm{max}} = 1 \cdot 10^{26}\,\mathrm{Pa{\cdot}s}$, $L = 100\,\mathrm{km}$, $t_p = 50\,\mathrm{Myr}$	2.890	33.0	27.104	173.92
$\eta_{\mathrm{max}} = 1 \cdot 10^{26}\,\mathrm{Pa{\cdot}s}$, $L = 200\,\mathrm{km}$	5.605	57.3	22.662	186.04
diffusion-dislocation creep	31.304	80.8	38.961	160.26
$T_{\mathrm{LAB}} = 1623\,\mathrm{K}$	11.012	46.6	30.077	134.97
$T_{\mathrm{LAB}} = 1623\,\mathrm{K}$, $t_p = 100\,\mathrm{Myr}$	5.661	31.6	30.517	132.16
$T_{\mathrm{LAB}} = 1623\,\mathrm{K}$, $t_p = 50\,\mathrm{Myr}$	3.435	31.6	27.523	160.48
$T_{\mathrm{LAB}} = 1623\,\mathrm{K}$, $T_p = 100\,\mathrm{K}$	6.582	43.8	27.673	153.00
$T_{\mathrm{LAB}} = 1623\,\mathrm{K}$, $T_p = 400\,\mathrm{K}$	14.370	40.2	33.396	117.52
$T_{\mathrm{LAB}} = 1623\,\mathrm{K}$, $d_{\mathrm{Asth}} = 100\,\mathrm{km}$	12.445	53.1	29.626	139.11
$T_{\mathrm{LAB}} = 1623\,\mathrm{K}$, $d_{\mathrm{Asth}} = 200\,\mathrm{km}$	9.533	41.2	30.329	132.70
$T_{\mathrm{LAB}} = 1623\,\mathrm{K}$, $L = 100\,\mathrm{km}$	13.282	41.7	35.407	117.32
$T_{\mathrm{LAB}} = 1623\,\mathrm{K}$, $L = 200\,\mathrm{km}$	8.279	50.7	25.481	158.14

Table S3. Overview of 2-D moving plate models used as data in Figure 4. Definitions as for Table S2.

Changed param.	Δq	Δh	q_0	L
– (reference case)	0.620	15.90	26.834	156.79
$v = 0.75\,\mathrm{cm/yr}$	0.974	21.13	26.478	164.60
$v = 3.0\,\mathrm{cm/yr}$	0.260	8.25	27.131	154.28
$\eta_j = [1 \cdot 10^{21}, 1 \cdot 10^{24}]\,\mathrm{Pa{\cdot}s}$	16.866	59.11	27.662	136.54
$\eta_j = [5 \cdot 10^{21}, 1 \cdot 10^{24}]\,\mathrm{Pa{\cdot}s}$	1.821	24.10	28.132	151.42
$\eta_j = [1 \cdot 10^{21}, 1 \cdot 10^{24}]\,\mathrm{Pa{\cdot}s}$	1.292	18.84	27.560	151.12
$\eta_j = [5 \cdot 10^{23}, 1 \cdot 10^{24}]\,\mathrm{Pa{\cdot}s}$	0.049	8.64	27.011	163.30
$E = 150\,\mathrm{kJ/mol}$	11.099	48.86	27.671	141.28
$E = 150\,\mathrm{kJ/mol}$, $v = 3.0\,\mathrm{cm/yr}$	15.721	33.47	37.081	99.87
$E = 150\,\mathrm{kJ/mol}$, $v = 0.75\,\mathrm{cm/yr}$	15.274	53.13	27.771	135.98
$E = 200\,\mathrm{kJ/mol}$	1.624	28.23	28.207	146.12
$T_p = 400\,\mathrm{K}$	1.170	19.95	26.806	159.50
diffusion-dislocation creep	1.338	27.29	27.121	162.03
$T_{\mathrm{LAB}} = 1623\,\mathrm{K}$	1.209	12.02	29.854	133.87
$T_{\mathrm{LAB}} = 1623\,\mathrm{K}$, $v = 0.75\,\mathrm{cm/yr}$	1.717	14.58	30.126	134.01
$T_{\mathrm{LAB}} = 1623\,\mathrm{K}$, $v = 3.0\,\mathrm{cm/yr}$	1.268	16.45	29.972	140.04
$T_{\mathrm{LAB}} = 1623\,\mathrm{K}$, diffusion-dislocation creep	1.650	18.94	31.002	128.98
$T_{\mathrm{LAB}} = 1623\,\mathrm{K}$, $\eta_j = [5 \cdot 10^{21}, 1 \cdot 10^{24}]\,\mathrm{Pa{\cdot}s}$	20.114	54.28	30.367	122.63
$T_{\mathrm{LAB}} = 1623\,\mathrm{K}$, $\eta_j = [5 \cdot 10^{21}, 1 \cdot 10^{24}]\,\mathrm{Pa{\cdot}s}$,$v = 3.0\,\mathrm{cm/yr}$	12.386	41.60	30.202	124.5
$T_{\mathrm{LAB}} = 1623\,\mathrm{K}$, $\eta_j = [5 \cdot 10^{21}, 1 \cdot 10^{24}]\,\mathrm{Pa{\cdot}s}$,$v = 0.75\,\mathrm{cm/yr}$	23.189	55.62	30.532	119.60
$T_{\mathrm{LAB}} = 1623\,\mathrm{K}$, $T_p = 300\,\mathrm{K}$	1.171	12.94	30.515	132.83
$T_{\mathrm{LAB}} = 1623\,\mathrm{K}$, $T_p = 350\,\mathrm{K}$	1.673	14.41	30.069	133.95
$T_{\mathrm{LAB}} = 1623\,\mathrm{K}$, $T_p = 400\,\mathrm{K}$	1.926	16.32	30.276	133.39
$T_{\mathrm{LAB}} = 1623\,\mathrm{K}$, $T_p = 450\,\mathrm{K}$	2.543	18.42	29.741	134.92
$T_{\mathrm{LAB}} = 1623\,\mathrm{K}$, $T_p = 300\,\mathrm{K}$, $v = 0.75\,\mathrm{cm/yr}$	2.283	16.98	29.716	136.93
$T_{\mathrm{LAB}} = 1623\,\mathrm{K}$, $T_p = 300\,\mathrm{K}$, $v = 3.0\,\mathrm{cm/yr}$	1.301	16.66	30.101	137.15
$T_{\mathrm{LAB}} = 1623\,\mathrm{K}$, $T_p = 400\,\mathrm{K}$, $v = 0.75\,\mathrm{cm/yr}$	3.056	22.30	29.833	138.57
$T_{\mathrm{LAB}} = 1623\,\mathrm{K}$, $T_p = 400\,\mathrm{K}$, $v = 3.0\,\mathrm{cm/yr}$	1.555	14.72	30.396	136.39

Table S4. Overview of 3-D moving plate models used as data in Figure 4. Definitions as for Table S2.

Changed param.	Δq	Δh	q_0	L
– (reference case)	1.983	30.21	26.761	161.11
$v = 0.75\,\mathrm{cm/yr}$	4.192	49.55	26.198	170.12
$v = 3.0\,\mathrm{cm/yr}$	0.761	18.23	27.609	153.73
$d_{\mathrm{Asth}} = 100\,\mathrm{km}$	1.248	21.00	27.012	158.34
$T_p = 150\,\mathrm{K}$	0.945	21.00	26.727	161.00
$T_p = 400\,\mathrm{K}$	5.284	50.93	26.753	163.39
$\eta_j = [5 \cdot 10^{21}, 1 \cdot 10^{24}]\,\mathrm{Pa{\cdot}s}$	3.446	34.70	28.583	148.52
$\eta_j = [5 \cdot 10^{23}, 1 \cdot 10^{24}]\,\mathrm{Pa{\cdot}s}$	0.275	9.75	26.685	162.65
$E = 150\,\mathrm{kJ/mol}$	8.148	48.91	31.198	143.04
$E = 200\,\mathrm{kJ/mol}$	4.566	40.95	28.481	148.76
$E = 300\,\mathrm{kJ/mol}$	0.333	12.03	26.449	165.58